# Combined Control of Machine & Grid Side Converters for PMSGs in Wind Energy Conversion Systems with Fast and Robust Performance


Saeid Gomroki
*Advanced Motion Systems Research Laboratory*
*School of ECE, College of Eng., University of Tehran*
Tehran, Iran
saeid.gomroki@ut.ac.ir

Sadegh Vaez-Zadeh
*Advanced Motion Systems Research Laboratory and Center of Excellence on Applied Electromagnetic Systems*
*School of ECE, College of Eng., University of Tehran*
Tehran, Iran
vaezs@ut.ac.ir

Alireza Jabbarnejad
*Advanced Motion Systems Research Laboratory*
*School of ECE, College of Eng., University of Tehran*
Tehran, Iran
jabbarnejad.a@ut.ac.ir



***Abstract*—Fast dynamics and smooth performance are important requirements that ensure the secure connection of wind energy conversion systems to the network according to grid codes. In this paper, a system model in grid voltage reference frame is developed. The combined control is then applied to both machine side and grid side converters of a grid-connected PMSG to fulfill the code requirements where the task of dc-link voltage control is assigned to the machine side converter. The control system enjoys low computation, simplicity, robustness and less dependency on grid parameters. Simulation results on a 1.5MW PMSG approve the performance superiority of the proposed control system in comparison with conventional control systems under different grid operating conditions.**



***Keywords—PMSG, combined control, power grid, renewable energy, power quality, switching frequency, sampling frequency***


## I. Introduction

Nowadays, the utilization of renewable energy sources, especially wind energy, has grown due to the increasing demand for electric power and climate change concerns. Voltage source converters (VSCs) based permanent magnet synchronous generators (PMSGs) with a full-scale back-to-back power converter are assessed to be more reliable and efficient than doubly-fed induction generators (DFIGs) [1]. There are several grid codes as requirements for connecting wind energy conversion systems (WECS) to the grid including fluctuation of voltage and harmonic distortion [2]. The control system plays an important role to meet these requirements.

The structure of WECS is divided into two separated parts: the machine side converter (MSC) and the grid side converter (GSC). The control of these parts has different tasks according to the grid codes. Generally, MSC is used to control the speed of the rotor to achieve maximum power generation and the grid side converter controls the dc-link voltage to balance exchanged power through dc-link. One of the most well-known methods for MSC control is vector control. In this method, the electromagnetic torque is controlled using the q-axis component of the stator current. In addition, the d-axis component is set to zero so as to obtain maximum torque per ampere (MTPA) [3]. The method has some merits, such as excellent steady-state performance and constant switching frequency. However, it has drawbacks including a moderate dynamic response, a high dependency on the machine parameters and tuning of PI controller gains. In direct torque control (DTC) as an alternative to vector control, the electromagnetic torque and stator flux linkage of generator are controlled directly using hysteresis controllers and a switching table [4]. It is known that the method enjoys a faster dynamic response and less dependency on machine parameters. Nevertheless, it suffers from high torque and current ripples, variable switching frequency, overstress on the turbine and acoustic noise. DTC-SVM is proposed to overcome these problems [5]. However, in comparison with the conventional DTC, it has some disadvantages including lower dynamic response, higher switching frequency, and online calculation. Base on the analogy between vector control and DTC, combined control is presented. It enjoys the smooth operation of VC under steady-state and fast response of DTC under transient state. This control method has been applied to AC electrical machines of different types [6,7]. Recently, this method is used to control PMSGs [8]. The control method has smoother performance compared to DTC plus faster dynamic response in comparison to vector control.

On the other hand, the most widely used control method for GSCs is vector control. In this method, active and reactive powers are regulated through the direct and quadrature grid currents, respectively [9]. The method has some advantages, such as lower total harmonic distortion (THD) of grid current, better power quality, and constant switching frequency. However, it has some disadvantages including a moderate dynamic response, a high dependence on the grid parameters and more computation time. Direct power control (DPC) is also applied to GSCs. The grid active and reactive powers are controlled directly [10]. The method has a faster dynamic response because of using a switching table instead of a PWM subsystem and less dependency on grid parameters. However, it suffers from high torque and current ripples and variable switching frequency. Furthermore, DPC based on space vector modulation (SVM) is presented. Compared to conventional DPC, this method has a lower grid current THD and a constant switching frequency. However, it suffers from the problem of tuning PI controllers and lower dynamic response [11]. Combined control is also applied to the GSC of DFIGs [12]. The method has a faster response than vector control but needs the tuning of PI controllers for regulating active and reactive powers, virtual flux estimation and two transformation blocks.

In this paper, the combined control is proposed for both MSC and GSC of PMSGs for the first time where the task of dc-link voltage control is assigned to the MSC. This full


XXX-X-XXXX-XXXX-X/XX/$XX.00 ©20XX IEEE

combined control has the same steady-state performance in addition to a faster dynamic response in comparison with conventional combined control [8]. Furthermore, it uses only one PI controller, which means that the tuning of controller gains is greatly reduced. Moreover, complex online calculations are avoided due to using a switching table instead of the PWM subsystem. Furthermore, the method has a lower parameter dependency due to the elimination of decoupling circuit. This paper has been organized as follows. In section II, system model is described followed by the control system in section III. In section IV, a comparison study between the vector control and the combined control methods is presented. In section V, the system simulation results are shown. Finally, the conclusion is presented in section VI.

## II. System Model

The overall system is depicted in Fig. 1. The wind generator is connected to the point of common coupling (PCC) through back-to-back VSCs. The converters operate in the following modes: a rectifier mode and an inverter mode. Furthermore, the two-level converter with IGBT switches is connected to the grid through a R-L filter as shown in Fig. 2. Model of the GSC is expressed as [9]:

$$\bar{e} = R_f \bar{i} + L_f \frac{di}{dt} + \bar{v} + j\omega_e L_f \bar{i} \tag{1}$$

where $\vec{e}$, $\vec{v}$ and $\vec{i}$ are grid voltage vector, output voltage vector of inverter and grid current vector, respectively. Also, $R_f$ and $L_f$ are output filter and $\omega_e$ is the grid angular frequency. In a grid voltage frame, the injected active and reactive powers to the grid are:

$$P_g = \frac{3}{2}\left(e_d i_d + e_q i_q\right), \tag{2}$$

$$Q_g = \frac{3}{2}\left(e_q i_d - e_d i_q\right). \tag{3}$$

In the rotating frame, the direct component of voltage is located on the horizontal axis. Consequently, the quadrature component of the grid voltage is equal to zero. The voltage of inverter can be expressed as:

$$V_{\alpha\beta} = \frac{2}{3} V_{dc} e^{j\frac{\pi}{3}(n-1)}, n = 1,2,...,6 \tag{4}$$

where $V_{dc}$ is the dc-link voltage of the inverter. On the other hand, the electromagnetic torque of PMSG is noted as [13]:

$$T_{em} = \frac{3}{2}\frac{P}{L_s}\lambda_s \lambda_m \sin(\delta). \tag{5}$$

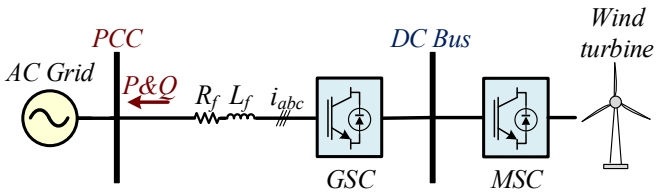


Fig. 1. Overview of WECS.

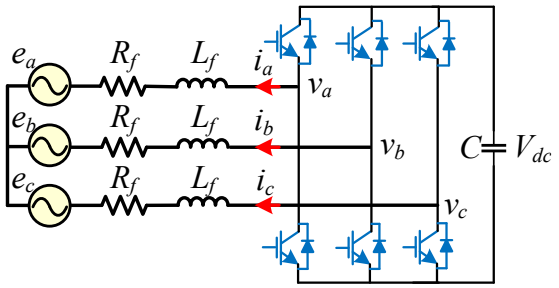


Fig. 2. Grid connected inverter with R-L filter.

where P, $L_s$, $\lambda_s$, $\lambda_m$ and δ are the number of pole pairs, stator inductance, stator flux linkage, rotor permanent magnet flux and the angle between stator and rotor flux.

## III. The Proposed Control System

In this section, the proposed control system for grid-connected PMSGs thorough back-to-back converters is presented.

### A. Control Principles

Here the basis of the combined control is outlined for MSC and GSC, respectively.

#### i. Machine Side Control

The electromagnetic torque deviation from (5) in the stator flux linkage rotary frame is defined as:

$$\Delta T_{em} = k_1 \Delta\lambda_x + k_2 \Delta\lambda_y, \tag{6}$$

where $k_1$ and $k_2$ are defined as:

$$k_1 = \frac{3}{2}\frac{P}{L_s}\lambda_m \sin(\delta), \tag{7}$$

$$k_2 = \frac{3}{2}\frac{P}{L_s}\lambda_m \cos(\delta). \tag{8}$$

Also, the machine electromagnetic torque based on stator current deviations can be expressed as:

$$\Delta T_{em} = k_3 \Delta i_x + k_4 \Delta i_y, \tag{9}$$

$$k_3 = \frac{3}{2} P\lambda_m \sin(\delta), \tag{10}$$

$$k_4 = \frac{3}{2} P\lambda_m \cos(\delta). \tag{11}$$

It can be concluded that:

$$\Delta\lambda_x \propto \Delta i_x, \tag{12}$$

$$\Delta\lambda_y \propto \Delta i_y. \tag{13}$$

These proportionalities confirm that DTC and VC perform the active and reactive power control of PMSGs in the same way through either current deviations or flux linkage

deviations. Thus, it is possible to exchange the flux linkage control and current control of DTC and VC respectively.

*ii. Grid Side Control*

If the voltage reference frame shown in Fig. 3 is considered, equation (2) and (3) are rewritten as:

$$P_g = \frac{3}{2} e_d i_d, \tag{14}$$

$$Q_g = -\frac{3}{2} e_d i_q. \tag{15}$$

The converter voltage in the grid voltage frame can be written in terms of dc-link voltage and converter switch status as:

$$V_d = \frac{2}{3} V_{dc} \cos\left(\omega_e t - \frac{\pi}{3}(n-1)\right), \tag{16}$$

$$V_q = -\frac{2}{3} V_{dc} \sin\left(\omega_e t - \frac{\pi}{3}(n-1)\right). \tag{17}$$

Equation (1) can be decomposed into the direct and quadrature components as:

$$e_d = R_f i_d + L_f \frac{di_d}{dt} + V_d - \omega_e L_f i_q, \tag{18}$$

$$e_q = R_f i_q + L_f \frac{di_q}{dt} + V_q + \omega_e L_f i_d. \tag{19}$$

Substituting (16) and (17) into (18) and (19) yields:

$$\frac{di_d}{dt} = \frac{2}{3L_f}\left[\frac{3}{2} e_d - V_{dc} \cos\left(\omega_e t - \frac{\pi}{3}(n-1)\right) - \frac{R_f P_g}{e_d} - \frac{\omega_e L_f Q_g}{e_d}\right], \tag{20}$$

$$\frac{di_q}{dt} = \frac{2}{3L_f}\left[V_{dc} \sin\left(\omega_e t - \frac{\pi}{3}(n-1)\right) + \frac{R_f Q_g}{e_d} - \frac{\omega_e L_f P_g}{e_d}\right]. \tag{21}$$

Based on the recent equations, it is concluded that by controlling GSC and applying the appropriate voltage vector, the grid current can be controlled. It should be noted that the hysteresis controllers are used to control the current components.

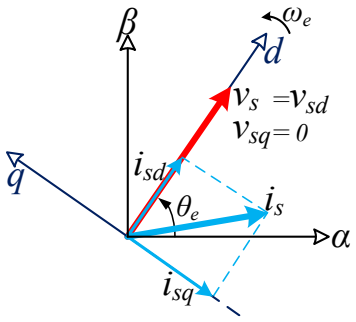


Fig. 3. Grid vector diagram in the rotary grid voltage frame.

*B. Control System Configuration*

In this subsection, the proposed control system is introduced. The combined control for MSC and GSC is shown in Fig. 4. The MSC is controlled in the stator flux linkage frame and the dc-link voltage regulation is used to control the electromagnetic torque by controlling stator quadrature current. To achieve MTPA, the direct component of stator current should be equal to zero. Flags of torque and flux linkage, in addition to the position of stator flux linkage are used to select the appropriate voltage vectors to apply to the generator. It should be noted that unlike the methods in which the GSC controls the dc-link voltage, this task is assigned to the MSC. The advantage here is that when a grid fault occurs, the voltage drop is felt faster and the generator power reduces to prevent sudden voltage surges in the dc-link voltage. A maximum power point tracking strategy is used and the generator active power is extracted from the generator speed. An optimum relationship-based (ORB) is needed for MPPT in which the wind speed measurement is not required [14]. It is important to note that if the power losses in the converters are ignored, then the generator power is equal to the injected grid power. The reference of reactive powers in both sides is considered equal to zero to keep the generator capacity free and reduce power losses in normal conditions. The direct and quadrature components of grid current are obtained from (14)

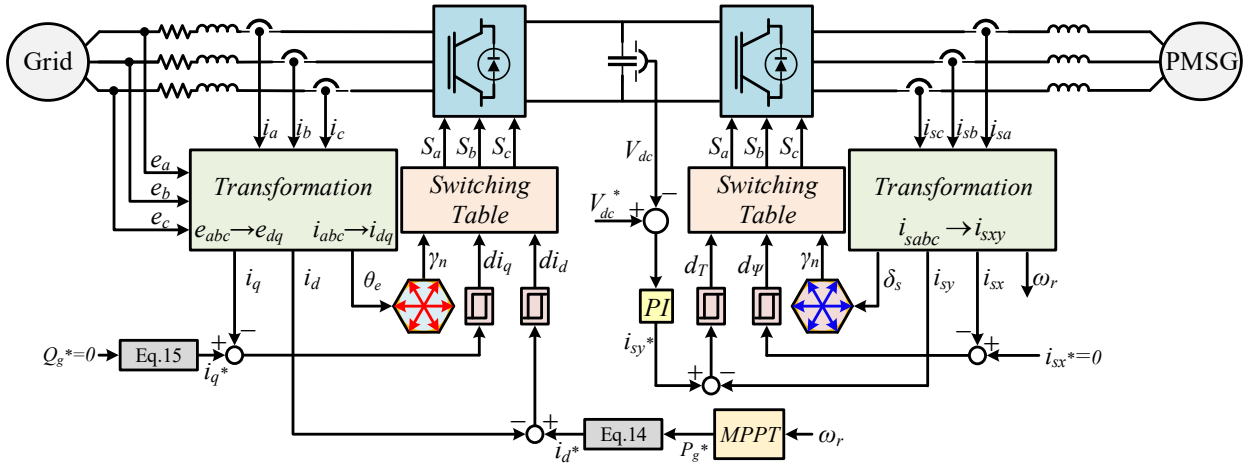


Fig. 4. Proposed control system.

and (15) and compared with the actual components in voltage frame. The errors are applied to the hysteresis controllers. The appropriate voltage vector is selected to apply to the grid side converter with the help of flags created and the position of the grid voltage vector. Injection active and reactive powers to the grid are controlled by controlling the components of the grid currents.

## IV. Performance Analysis

In this section, a comparison between the vector control method and the combined control method of this paper is presented from a new perspective. The comparison consists of two parts. The first part is carried out under the same switching frequency for both methods. However, the second part is performed under different switching frequencies depending on the requirements of each method.

Sampling frequency is an important factor determining control performance and system switching frequency. The sampling frequency (1/Ts) is equal to carrier wave frequency for vector control method as shown in Fig. 5 (a). Three voltage vectors containing two active and one zero vector are selected in each $T_s$ in this method. Therefore, the active power remains within the permitted range shown with ΔP/2 around $P^*$ by applying these vectors as shown in Fig 5 (a). On the other hand, a similar analysis is carried out for the combined control method as shown in Fig. 5 (b) [15]. In order to achieve the switching frequency of the combined control method as high as the switching frequency of the vector control, the sampling frequency of the combined control method is increased. Since a voltage vector is applied at each sampling interval, the number of voltage vectors increases which provides higher power quality and lower current THD. Therefore, in the combined control method, more voltage vectors are applied to the converter than the vector control method resulting in lower power ripples. It should be noted that vector control method needs to operate in a relatively high frequency. The reason is that the output waveform approaches the appropriate shape and produces harmonics far beyond the main frequency to reduce the output filter size. It can also be said that the frequency of these methods is constant. In contrast, the combined control method operates at a lower and variable frequency. The reason is that the instantaneous frequencies are higher than the average frequency in this method. In addition, a high switching frequency causes higher losses and a lower lifetime of switches [16]. Another comparison is also carried out at an unequal switching frequency as shown in Fig 5 (c). In this situation, the sampling frequency of the combined control method is lower than that of the previous combined control methods which leads to lower switching frequency for the combined control method. Consequently, the number of voltage vectors that are applied to the converter decreases in each $T_s$. Thus, power quality deteriorates with respect to that under vector control method.

## V. Simulation Results

In this section, firstly, the steady-state performance of WECS under the proposed combined-combined (CC) control method is compared with those under vector-vector (VV) and combined-vector (CV) control methods under different switching frequencies for vector and combined control. Then the comparison is repeated for CC and VV control methods with the same switching frequency for vector and combined control. Finally, the transient performance of the proposed method in comparison with other methods is investigated. The simulation studies are carried out for a 1.5MW non-salient PMSG-based WECS using MATLAB/Simulink [17].

The simulation results for the electromagnetic torque, active power, reactive power and dc-link voltage under unequal frequency are depicted in Fig. 6. In addition, switching frequency for vector control and combined control on each side is considered as 7.5 kHz and 3 kHz respectively. It is seen that VV method has a better performance than CV and CC methods in terms of lower ripples. Moreover, the THD of current signals and power ripples of the generator side are almost the same under CV and CC methods due to the similarity of the switching logic.

Then, the comparison is carried out with the same switching frequency for VV and CC methods in Fig. 7. According to the previous section, it can be found that CC has better performance than VV under the same switching frequency in terms of signal ripples. Finally, Fig. 8 shows the transient performance of the control methods. At 0.1 and 0.15 seconds, a local load with a capacity of one-third of the rated capacity is connected and then disconnected, respectively. At these conditions, the dc-link voltage drops due to the sudden increase in the power demand and the high inertia of the generator. Therefore, the dc-link supplies the demand instantly at the cost of its voltage drop.

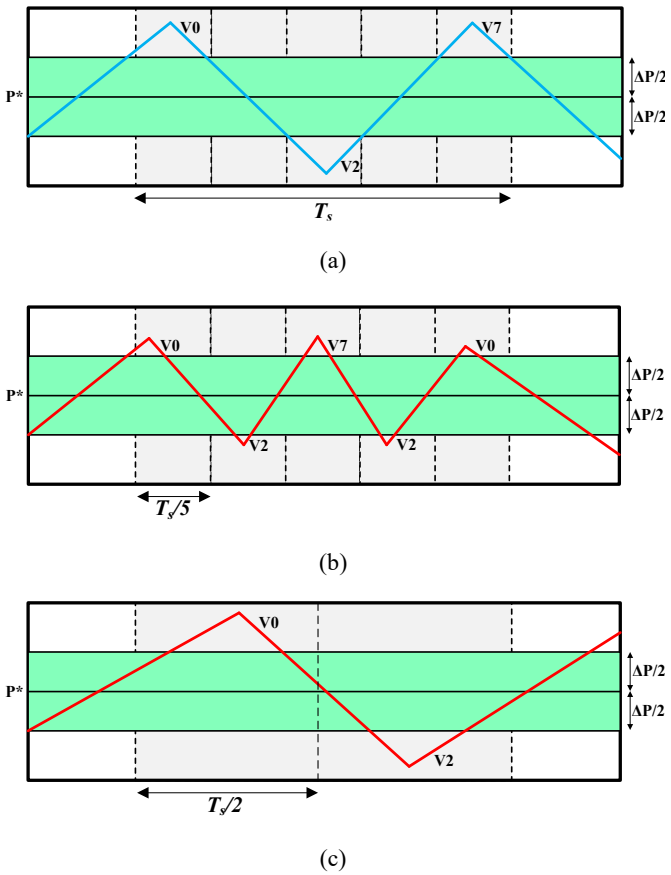


Fig. 5. Switching logic in control methods; a) Vector control, b) Combined control with the same frequency, c) Combined control with the separated frequency.

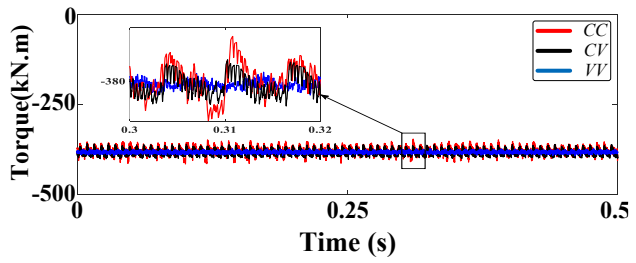


(a)

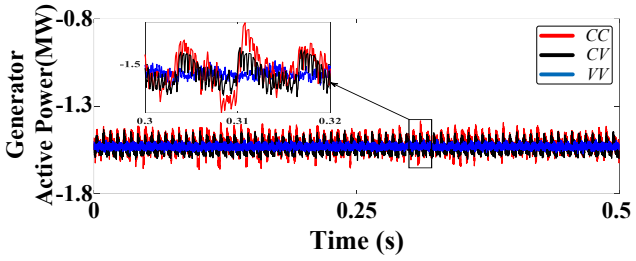


(b)

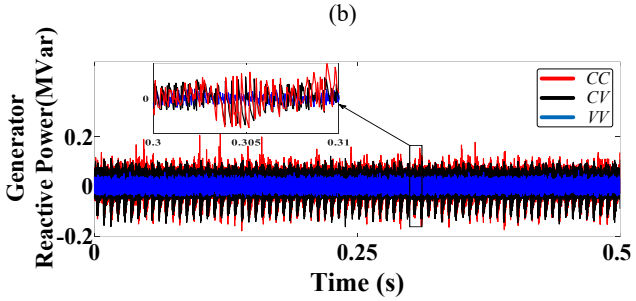


(c)

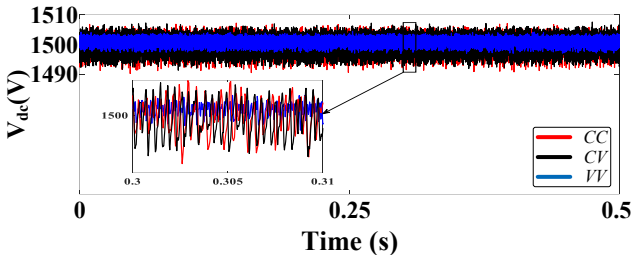


(d)

Fig. 6. Simulation results for the separated switching frequency; a) Electromagnetic torque, b) Machine active power, c) Machine reactive power, d) dc-link voltage.

Then the generator active power increases to charge the dc-link again and supply the local load. The proposed control has fast and robust performance against severe load changing according to Fig 8. The quality of control signals of the grid side is almost the same under CV and VV methods due to the similarity in the switching logic. The comparative analysis of control methods is summarized in Table I.

## VI. Conclusion

In this paper, the combined control method is applied to both machine and grid side converters of PMSGs. The performance merits of the control is confirmed by comparing

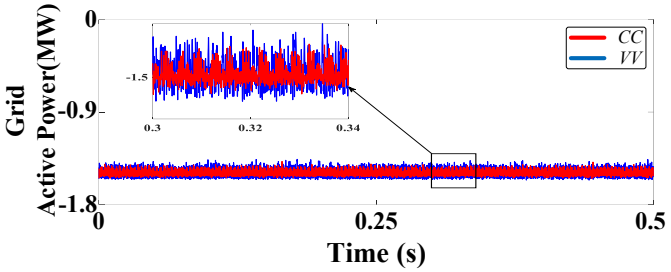


(a)

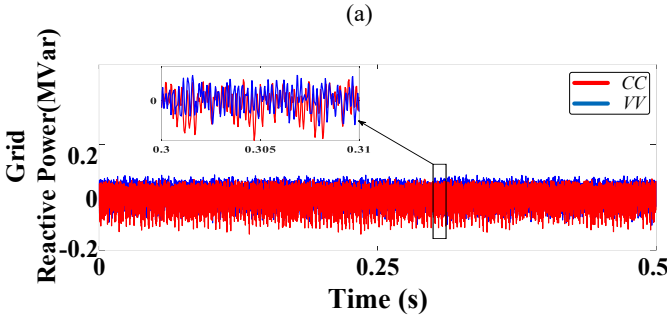


(b)

Fig. 7. Simulation results for the same switching frequency; a) Grid active power, b) Grid reactive power.

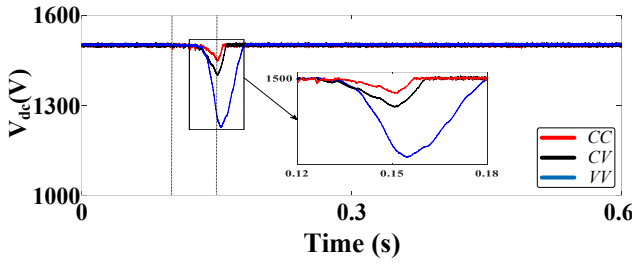


(a)

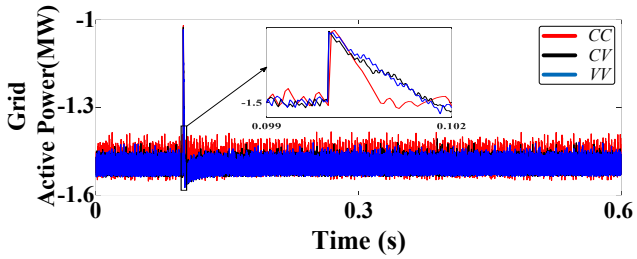


(b)

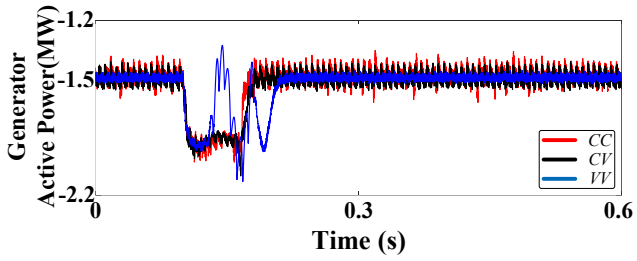


(c)

Fig. 8. Simulation results for transient response; a) dc-link voltage, b) Grid active power, c) Machine active power.

the method with the methods in which a vector control is applied to the grid side converter, with a machine side converter under either a vector or a combined control method. The proposed full combined control provides faster performance due to using a PI controller only. In addition, it causes a lower dc-link voltage drop. Thus, accommodating a better performance under fault conditions.

TABLE I. COMPARATIVE RESULTS BASED ON TYPE OF CONTROL

| | VV | CV | CC[a] |
|---|---|---|---|
| $V_{dc}$ ripple | Low | Medium | Medium |
| Grid current THD | Low | Low | Medium |
| Machine current THD | Low | Medium | Medium |
| PWM subsystem | two | one | zero |
| Simplicity | Complex | Simple | Simpler |
| Transient Response | Slow | Fast | Faster |
| Robustness | Low | Medium | High |
| No. of PI controllers | 4 | 2 | 1 |

[a.] Proposed Control

## REFERENCES


[1] F. Blaabjerg, Z. Chen, and S. B. Kjaer, "Power electronics as efficient interface in dispersed power generation systems," *IEEE Transactions on Power Electronics,* vol. 19, no. 5, pp. 1184-1194, 2004.

[2] M. Mohseni and S. M. Islam, "Review of international grid codes for wind power integration: diversity, technology and a case for global standard," *Renewable and Sustainable Energy Reviews,* vol. 16, no. 6, pp. 3876-3890, 2012.

[3] S. Li, T. A. Haskew, R. P. Swatloski, and W. Gathings, "Optimal and direct-current vector control of direct-driven PMSG wind turbines," *IEEE Transactions on Power Electronics,* vol. 27, no. 5, pp. 2325-2337, 2011.

[4] L. Zhong, M. F. Rahman, W. Y. Hu, and K. Lim, "Analysis of direct torque control in permanent magnet synchronous motor drives," *IEEE Transactions on Power Electronics,* vol. 12, no. 3, pp. 528-536, 1997.

[5] Z. Zhang, Y. Zhao, W. Qiao, and L. Qu, "A space-vector-modulated sensorless direct-torque control for direct-drive PMSG wind turbines," *IEEE Transactions on Industry Applications,* vol. 50, no. 4, pp. 2331-2341, 2014.

[6] E. Daryabeigi and S. Vaez-Zadeh, "A combined control for fast and smooth performance of IPM motor drives over wide operating conditions," *IEEE Transactions on Energy Conversion,* vol. 33, no. 3, pp. 1384-1391, 2018.

[7] J. Mohammadi, S. Vaez-Zadeh, S. Afsharnia, and E. Daryabeigi, "A combined vector and direct power control for DFIG-based wind turbines," *IEEE Transactions on Sustainable Energy,* vol. 5, no. 3, pp. 767-775, 2014.

[8] M. Jahanpour-Dehkordi, S. Vaez-Zadeh, and J. Mohammadi, "Development of a combined control system to improve performance of a PMSG based wind energy conversion system under normal and grid fault conditions," *IEEE Transactions on Energy Conversion,* vol. 34, no. 3, pp. 1287-1295, 2019.

[9] M. Chinchilla, S. Arnaltes, and J. C. Burgos, "Control of permanent-magnet generators applied to variable-speed wind-energy systems connected to the grid," *IEEE Transactions on Energy Conversion,* vol. 21, no. 1, pp. 130-135, 2006.

[10] T. Noguchi, H. Tomiki, S. Kondo, and I. Takahashi, "Direct power control of PWM converter without power-source voltage sensors," *IEEE Transactions on Industry Applications,* vol. 34, no. 3, pp. 473-479, 1998.

[11] M. Allagui, O. B. Hasnaoui, and J. Belhadj, "A 2MW direct drive wind turbine; vector control and direct torque control techniques comparison," *Journal of Energy in Southern Africa,* vol. 25, no. 2, pp. 117-126, 2014.

[12] J. Mohammadi, S. Vaez-Zadeh, E. Ebrahimzadeh, and F. Blaabjerg, "Combined control method for grid-side converter of doubly fed induction generator-based wind energy conversion systems," *IET Renewable Power Generation,* vol. 12, no. 8, pp. 943-952, 2018.

[13] S. Vaez-Zadeh, *Control of permanent magnet synchronous motors*. Oxford University Press, 2018.

[14] Y. Xia, K. H. Ahmed, and B. W. Williams, "A new maximum power point tracking technique for permanent magnet synchronous generator based wind energy conversion system," *IEEE Transactions on Power Electronics,* vol. 26, no. 12, pp. 3609-3620, 2011.

[15] J.-W. Kang and S.-K. Sul, "Analysis and prediction of inverter switching frequency in direct torque control of induction machine based on hysteresis bands and machine parameters," *IEEE Transactions on Industrial Electronics,* vol. 48, no. 3, pp. 545-553, 2001.

[16] Y. Korkmaz, F. Korkmaz, I. Topaloglu, and H. Mamur, "Comparing of switching frequency on vector controlled asynchronous motor," *arXiv preprint arXiv:1610.03175,* 2016.

[17] M. Nasiri, J. Milimonfared, and S. Fathi, "A review of low-voltage ride-through enhancement methods for permanent magnet synchronous generator based wind turbines," *Renewable and Sustainable Energy Reviews,* vol. 47, pp. 399-415, 2015.